Published in final edited form as:
Science. 2011 July 22; 333(6041): 456–459. doi:10.1126/science.1203963.

Cilia-Like Beating of Active Microtubule Bundles

Timothy Sanchez[1], **David Welch**[2], **Daniela Nicastro**[3], and **Zvonimir Dogic**[1,*]

[1]Department of Physics, Brandeis University, 415 South Street, Waltham, MA 02454, USA

[2]Graduate Program in Biophysics and Structural Biology, Brandeis University, 415 South Street, Waltham, MA 02454, USA

[3]Department of Biology, Brandeis University, 415 South Street, Waltham, MA 02454, USA

Abstract

The mechanism that drives the regular beating of individual cilia and flagella, as well as dense ciliary fields, remains unclear. We describe a minimal model system, composed of microtubules and molecular motors, which self-assemble into active bundles exhibiting beating patterns reminiscent of those found in eukaryotic cilia and flagella. These observations suggest that hundreds of molecular motors, acting within an elastic microtubule bundle, spontaneously synchronize their activity to generate large-scale oscillations. Furthermore, we also demonstrate that densely packed, actively bending bundles spontaneously synchronize their beating patterns to produce collective behavior similar to metachronal waves observed in ciliary fields. The simple in vitro system described here could provide insights into beating of isolated eukaryotic cilia and flagella, as well as their synchronization in dense ciliary fields.

New behavior frequently emerges as complex structures are assembled from simpler components. In biology, an example of such hierarchical organization is the axoneme—the core structure of eukaryotic cilia and flagella (1). Important building blocks of axonemes are dynein motors, which convert energy from adenosine triphosphate (ATP) hydrolysis into linear movement along a microtubule (MT) track (2). In each axoneme, dyneins are assembled onto a scaffold of nine cylindrically arranged doublet MTs. Dyneins are bound to one doublet MT through an ATP-insensitive cargo-binding site while moving in an ATP-dependent manner along the neighboring MT. This causes sliding of neighboring doublet MTs against each other, which is thought to be subsequently converted into bending by elastic connectors that restrict intermicrotubule sliding (3, 4). The activity of thousands of dyneins within each axoneme is regulated to form oscillatory beating patterns, an emergent behavior that is qualitatively different from the linearly moving isolated dynein motors. However, the exact mechanism that causes the formation of self-sustained beating patterns of isolated axonemes remains unclear (5). At the next level of hierarchy, axonemes are the essential building blocks of dense ciliary fields, where thousands of individual cilia beat in a tightly coordinated fashion. In these arrays, the neighboring cilia are not in identical states of their beat cycle but are offset by a well-defined phase shift, generating regions of higher density that travel as metachronal waves and are capable of either propelling entire cells or moving fluid across the surface of various tissues. Metachronal waves are critical for a

*To whom correspondence should be addressed. zdogic@brandeis.edu.

Supporting Online Material
www.sciencemag.org/cgi/content/full/333/6041/456/DC1
Materials and Methods
Figs. S1 to S3
References
Movies S1 to S10

variety of processes, including the motility of ciliated protists, mucus clearance by airway cilia, and the determination of the left/right symmetry during embryonic development in humans (6, 7). Defective cilia are associated with severe human diseases (6). Previous studies of axoneme beating have primarily used a top-down approach by deconstructing a functional organelle in order to identify the functional components required for beating (8–11). Here, using a bottom-up approach, we identify a few essential components required for an assembly of active MT bundles, a simple biological oscillator whose beating patterns are reminiscent of isolated cilia. This minimal in vitro system is similar to previously proposed theoretical models of cilia and flagella (12, 13). Furthermore, we also demonstrate that dense fields of interacting active MT bundles exhibit synchronous beating behavior similar to metachronal waves observed in ciliary fields (14, 15).

The assembly of oscillatory active bundles requires three main components (Fig. 1A). The first two, biotin-labeled kinesin motors bound into clusters through multimeric streptavidin and taxol-stabilized MTs, spontaneously organize into asterlike structures, reminiscent of mitotic spindles (16, 17). The kinesin clusters simultaneously bind and walk along two neighboring MTs, resulting in their relative displacement (“inter-MT sliding”). Addition of a third component, nonadsorbing polymer polyethylene glycol (PEG), alters the behavior of the system and leads to the assembly of oscillating bundles. PEG induces attractive interactions between MTs through the depletion mechanism (fig. S1), leading to their bundling (18). Having MTs side by side greatly increases the probability of kinesin clusters simultaneously binding and walking along neighboring MTs. The relative motion of MTs in these bundles depends on their polarity; whereas motor clusters generate displacement between MTs of opposite polarity, no displacement is induced between MTs with the same polarity (19).

To assemble self-oscillating MT bundles, we flowed the MT/kinesin/PEG mixture into a flow chamber coated with a polymer brush to avoid motility due to surface-bound motors (20). In the bulk of the sample, the active MT network contracted into asterlike structures (16, 17); however, a number of bundles remained attached to the edges of the flow chamber or partially trapped under air bubbles, and thus separated from the bulk of the contracting structures. Once separated, these bundles exhibited uniform large-scale beating patterns (Fig. 1, B and C, fig. S2, and movies S1 to S3). To ensure that background MTs did not interfere with the beating patterns, in some experiments we displaced the unbound MT/kinesin mixture with a buffer containing only ATP, PEG, and kinesin clusters (but no MTs). In these samples, the attached bundles continued to beat for more than 1 hour. The primary factor that determines the beating frequency is the length of the bundle, which can range from less than 10 μm to more than 100 μm, with longer bundles beating with longer periods (fig. S3). We hypothesize that active bundles contain MTs with mixed polarity and that the oscillatory beating is driven by the activity of kinesin clusters that induce interfilament sliding. At the same time, the osmotic pressure due to PEG keeps the bundle together and, in combination with the attachment at the base, transforms the sliding motion into local bending, producing large-scale beating patterns.

How does the minimal system of active bundles compare with biological axonemes? Although both have a scaffold composed of MTs, cilia and flagella are highly ordered structures that contain more than 650 different proteins (8). In contrast, active bundles are disorganized structures of varying size that only contain MTs and kinesin clusters. Active MT bundles exhibit oscillations only when attached to a fixed boundary, similarly to axonemes that are attached to the cell cytoskeleton through the basal body (21). Additionally, both active bundles and axonemes contain molecular motors that drive interfilament sliding. However, in axonemes, dynein motors are permanently attached to one doublet MT (in an ATP-insensitive manner), while walking on a neighboring doublet in an

ATP-dependent manner (4). In contrast, the in vitro MT bundles are driven by kinesin clusters, which considerably differ from axonemal dyneins in size and direction, as well as other aspects (22), including that kinesin clusters continuously associate and dissociate from active bundles because they lack permanent attachment sites to MTs.

Another requirement for the generation of active oscillations in both systems is the presence of condensing agents that arrange MTs into bundles and also might restrict MT sliding. In axonemes, specialized structures, such as the nexin link, cross-link the nine MT doublets (11). It has been suggested that the nexin binds, dissociates, and rebinds neighboring MT doublets, thus allowing them to slide past each other over a significant distance while maintaining a well-defined separation (23). In depletion-driven bundling, it is not obvious if individual MTs slide freely past each other or remain fixed in a more static structure due to large interfilament friction. The latter was found to be the case for depletion-driven bundling of actin filaments (24, 25). Using a recently developed method, we investigated the dynamics of MT bundles confined to quasi–two-dimensional (2D) chambers and found that MTs slide freely past each other, indicating a relatively low interfilament friction (Fig. 2, A and B, and movie S4) (24). We measured the mean square displacement (MSD) between two MTs as a function of time (Fig. 2C). Purely viscous coupling would result in an MSD curve that increases linearly over time with a slope of 1 on a log-log plot (red curve in Fig. 2C). However, the measured MSD curves exhibited subdiffusive behavior, indicating that the coupling between MTs has weak elastic as well as a viscous component (black curve in Fig. 2C). In active bundles, an additional source of interfilament friction might arise from the motor proteins themselves (26). The relative importance of viscous and elastic interactions in MT bundles for the formation of beating patterns will have to be examined in more detail in future studies. Interestingly, the above-described four requirements for beating of active bundles, i.e., (i) microtubule tracks, (ii) motor complexes interacting with at least two microtubules, (iii) boundary attachment, and (iv) linkages permitting interfilament sliding, are almost identical to the main ingredients of previously proposed theoretical models of cilia and flagella (12, 13).

A major difference between active bundles and biological cilia and flagella is the significantly slower beating frequency observed in the in vitro system. In light of the marked differences in length, width, motors, and MT organization, this difference is not too surprising. A likely factor contributing to the slower beating is the arrangement of the motors on the MTs. In cilia and flagella, the motors are densely packed along the doublets [20 motors per 100 nm (11)], and they are fixed to one MT while walking on the neighboring one, whereas in the in vitro system, motors continuously walk, associate, and dissociate from both MTs.

In addition to exploring the behavior of isolated active MT bundles, our model system also assembles into dense arrays, enabling us to study the emergent behavior that arises from interactions between actively beating bundles (movies S5 to S8). At sufficiently high density, active bundles spontaneously synchronize to generate metachronal waves similar to those observed in native ciliary fields. Although the base of each active MT bundle remains stationary, successive phase shifts in their beat cycles generate regions of higher MT bundle density that spontaneously propagate along the interface at a well-defined velocity (Fig. 3 and movie S7). Along an air-water interface, several regions of synchronous beating could be distinguished, in which metachronal waves traveled in either a clockwise or counterclockwise direction as seen in a kymograph in Fig. 3D. In a few cases, collective metachronal waves were capable of transporting passive material (movie S9), similar to the transport of food particles by ciliated protists or mucus by ciliated epithelia. Although all active bundles were lodged onto the coverslip at the edge of an air-water interface, bundles were observed in focus at *z* positions away from the chamber surface, indicating 3D beating

patterns (movie S10). The qualitative behavior of this self-assembled active system at an air-water interface is similar to that of biological ciliary fields (compare Fig. 3, C and E). In native systems, however, metachronal waves travel typically over large regions with the same handedness (Fig. 3E).

The metachronal waves of the artificial system were quantitatively analyzed in Fig. 4. The 3D spatial-temporal correlation function shown in Fig. 4A indicates that the wavelength of the metachronal waves was 54 μm, the temporal frequency is 4.9×10^{-3} Hz, and the velocity is 0.27 μm/sec. By comparison, the ciliary field of the *Opalina ranarum* produces metachronal waves with a spatial wavelength of 17 μm, a temporal frequency of 3 Hz, and a velocity of 51 μm/sec. It has been proposed that the highly coordinated behavior of ciliary fields is not controlled by chemical signaling pathways but merely arises from hydrodynamic coupling between neighboring cilia (14, 15). Our observation of metachronal waves in a simplified in vitro system supports this hypothesis.

In conclusion, we have demonstrated that a simple nonequilibrium system, composed of MTs and molecular motors, spontaneously synchronizes on multiple levels of hierarchy, with qualitatively new functions emerging at each hierarchical level. This system should provide insight into the mechanisms that drive the oscillations of biological nanomachines (27–30), while simultaneously enabling assembly of active materials capable of fluid transport and swimming motion (31, 32).

Supplementary Material

Refer to Web version on PubMed Central for supplementary material.

Acknowledgments

We acknowledge useful discussions with S. Fraden and M. Hagan. We are grateful to J. Chung and J. Gelles for their help in purification of microtubules and kinesin and also acknowledge D. Chen and E. Peck for images of beating *Chlamydomonas reinhardtii*. We are thankful to the IWF for their permission to use images of *Opalina ranarum* (Fig. 3C). This work was supported by funding from the W. M. Keck Foundation, National Science Foundation (DMR-MRSEC-0820492), and National Institutes of Health (5K25GM85613 to Z.D. and 5R01GM083122 to D.N.).

References and Notes

1. Bray, D. Cell Movements: From Molecular to Motility. Garland Publishing; New York: 2000.
2. Reck-Peterson SL, et al. Cell. 2006; 126:335. [PubMed: 16873064]
3. Satir P. J Cell Biol. 1968; 39:77. [PubMed: 5678451]
4. Summers KE, Gibbons IR. Proc Natl Acad Sci USA. 1971; 68:3092. [PubMed: 5289252]
5. Brokaw CJ. Cell Motil Cytoskeleton. 2009; 66:425. [PubMed: 18828155]
6. Afzelius BA. J Pathol. 2004; 204:470. [PubMed: 15495266]
7. Okada Y, Takeda S, Tanaka Y, Belmonte JCI, Hirokawa N. Cell. 2005; 121:633. [PubMed: 15907475]
8. Pazour GJ, Agrin N, Leszyk J, Witman GB. J Cell Biol. 2005; 170:103. [PubMed: 15998802]
9. Stolc V, Samanta MP, Tongprasit W, Marshall WF. Proc Natl Acad Sci USA. 2005; 102:3703. [PubMed: 15738400]
10. Dymek EE, Smith EF. J Cell Biol. 2007; 179:515. [PubMed: 17967944]
11. Heuser T, Raytchev M, Krell J, Porter ME, Nicastro D. J Cell Biol. 2009; 187:921. [PubMed: 20008568]
12. Jülicher F, Prost J. Phys Rev Lett. 1997; 78:4510.
13. Camalet S, Jülicher F, Prost J. Phys Rev Lett. 1999; 82:1590.
14. Guirao B, Joanny JF. Biophys J. 2007; 92:1900. [PubMed: 17189311]

15. Gueron S, Levit-Gurevich K. Proc Natl Acad Sci USA. 1999; 96:12240. [PubMed: 10535905]
16. Nédélec FJ, Surrey T, Maggs AC, Leibler S. Nature. 1997; 389:305. [PubMed: 9305848]
17. Surrey T, Nedelec F, Leibler S, Karsenti E. Science. 2001; 292:1167. [PubMed: 11349149]
18. Needleman DJ, et al. Phys Rev Lett. 2004; 93:198104. [PubMed: 15600887]
19. Hentrich C, Surrey T. J Cell Biol. 2010; 189:465. [PubMed: 20439998]
20. Materials and methods are available as supporting material on *Science* Online.
21. Gibbons BH, Gibbons IR. J Cell Biol. 1972; 54:75. [PubMed: 4261039]
22. Vale RD. Cell. 2003; 112:467. [PubMed: 12600311]
23. Minoura I, Yagi T, Kamiya R. Cell Struct Funct. 1999; 24:27. [PubMed: 10355876]
24. Lau AWC, Prasad A, Dogic Z. EPL. 2009; 87:48006.
25. Claessens MM, Bathe M, Frey E, Bausch AR. Nat Mater. 2006; 5:748. [PubMed: 16921360]
26. Bormuth V, Varga V, Howard J, Schäffer E. Science. 2009; 325:870. [PubMed: 19679813]
27. Plaçais PY, Balland M, Guérin T, Joanny JF, Martin P. Phys Rev Lett. 2009; 103:158102. [PubMed: 19905668]
28. Guérin T, Prost J, Martin P, Joanny JF. Curr Opin Cell Biol. 2010; 22:14. [PubMed: 20074926]
29. Gittes F, Meyhöfer E, Baek S, Howard J. Biophys J. 1996; 70:418. [PubMed: 8770218]
30. Brangwynne CP, Koenderink GH, Mackintosh FC, Weitz DA. Phys Rev Lett. 2008; 100:118104. [PubMed: 18517833]
31. Dreyfus R, et al. Nature. 2005; 437:862. [PubMed: 16208366]
32. Vilfan M, et al. Proc Natl Acad Sci USA. 2010; 107:1844. [PubMed: 19934055]
33. Horstmann, E. IWF movie “C792/1959”: Flimmerepithel. Institut fuer den Wissenschaftlichen Film; Goettingen: 1964.

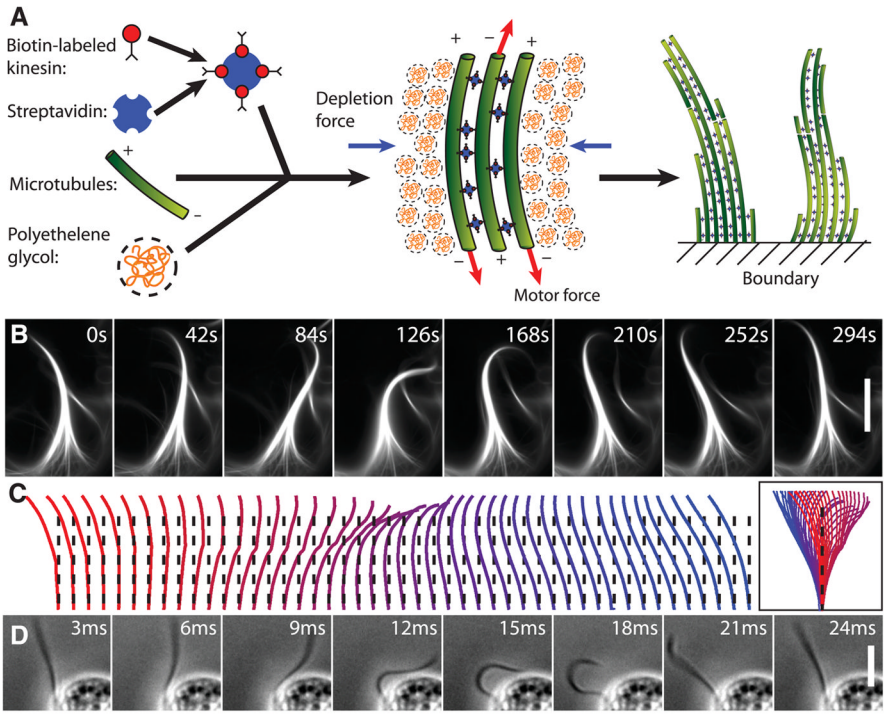

Fig. 1.

A minimal system of MTs, molecular motors, and depleting polymer assembles into actively beating MT bundles. (**A**) Schematic illustration of all components required for assembly of active bundles. (**B**) A sequence of images illustrating the beating pattern of an active bundle over one beat cycle. Scale bar, 30 μm. (**C**) The conformation of the bending MT bundle indicates a fairly symmetric beating pattern that is reminiscent of those found in cilia and flagella. (**D**) Sequence of images showing one beating cycle of a flagellum from *Chlamydomonas reinhardtii*. Scale bar, 5 μm.

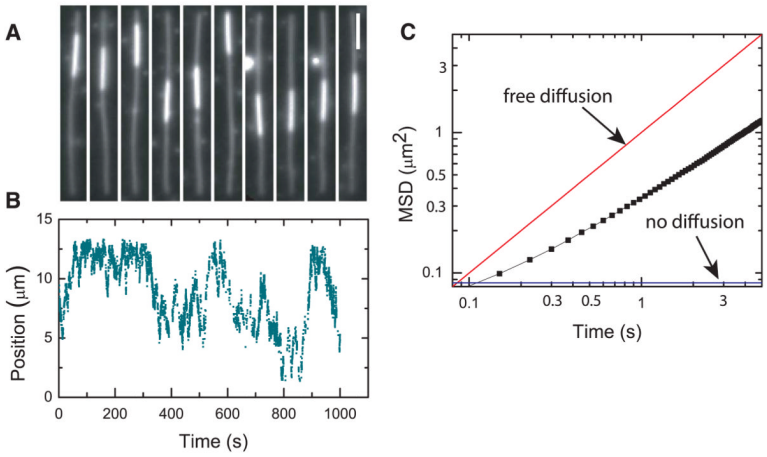

Fig. 2.

A short MT bound to a longer filament by the depletion force exhibits thermally driven sliding motion. (**A**) A time-lapse observation of two sliding MTs over a period of 15 min. Scale bar, 3 μm. At this depletant concentration, unbinding events are very rare. (**B**) A trajectory of a shorter MT diffusing while bound to the longer MT. The position is measured relative to the end point of a longer MT. (**C**) MSD of the relative diffusion between the two MTs. The subdiffusive behavior indicates viscoelastic coupling between the two filaments. The MSD data are averaged for six filament pairs in which shorter filaments were between 3 and 4 μm long. In each case, the dynamics were observed for anywhere between 10 and 30 min.

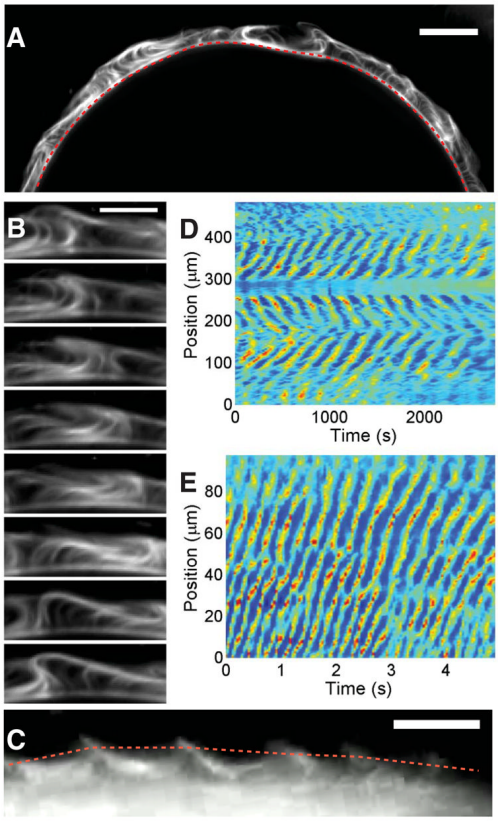

Fig. 3.

Propagation of metachronal waves in a densely packed array of active MT bundles. (**A**) Interface of an air bubble covered with a dense monolayer of beating bundles (see also movie S7). The bundles are trapped at their bases between the glass and an air bubble. Regions of the edge that are covered with a sufficiently high density of active MT bundles exhibit methachronal traveling waves. The length of bundles is ~10 μm. Scale bar, 40 μm. (**B**) Time sequence (25-s time lapse) of one section from (A) shows local propagation of metachronal waves. Scale bar, 20 μm. (**C**) Image of a ciliary field on the cell surface of the ciliate *Opalina ranarum*, which generates traveling metachronal waves. Scale bar, 20 μm. (**D**) A kymograph of the fluorescence intensity represents the local MT density of the bundle field, with higher densities displayed in red and lower densities in blue. Easily distinguishable metachronal waves travel in either a clockwise or counterclockwise direction at different regions of interface. Low surface coverage at the top of the interface results in asynchronous beating of active bundles. Dashed red line in (A) indicates the position at which the kymograph was taken. (**E**) A kymograph of the ciliate field shown in (C) is presented for comparison. Dashed red line in (C) indicates the position at which the kymograph was taken. [With permission from IWF gGMBH, images in (C) and (E) are extracted from (33).]

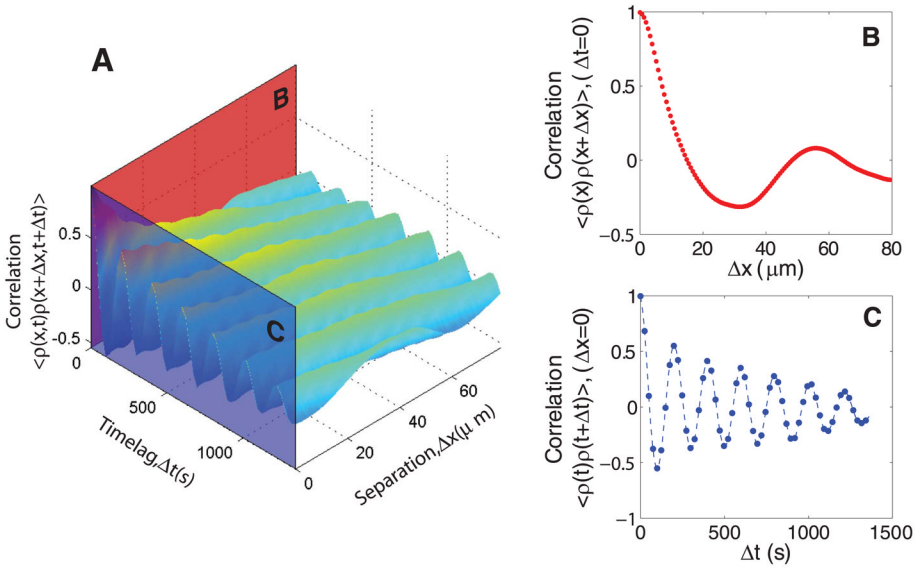

Fig. 4.

Quantitative analysis of the spatial and temporal properties of a travelling metachronal wave. (**A**) A 3D plot of the correlation function of the density, ρ, is plotted as a function of spatial separation (Δ*x*) and temporal time lag (Δ*t*). (**B**) The spatial correlation function at zero time lag (Δ*t* = 0) corresponds to the red slice of the 3D surface plot in (A). The functional form indicates a periodic structure with a wavelength of 54 μm. (**C**) The temporal autocorrelation plot corresponds to the blue slice of the surface plot in (A) at zero spatial separation (Δ*x* = 0). The periodicity of this correlation highlights the time propagation of the density wave, as each point becomes anticorrelated with itself when 1/2 of a wavelength has passed and correlated once again when a full wavelength has passed.